# *Measurement of Air Entrainment During Pouring of an Aluminum Alloy*

**Francisco V. Guerra, Lucas Archer, Richard A. Hardin & Christoph Beckermann**

**Metallurgical and Materials Transactions B**

ISSN 1073-5615
Volume 52
Number 1

Metall Mater Trans B (2021) 52:123-137
DOI 10.1007/s11663-020-01998-3

Springer

# Measurement of Air Entrainment During Pouring of an Aluminum Alloy

FRANCISCO V. GUERRA, LUCAS ARCHER, RICHARD A. HARDIN, and CHRISTOPH BECKERMANN

Understanding and reducing air entrainment in liquid metals is important for improving casting filling systems and liquid metal transfer processes. Air entrainment generates oxide inclusions that reduce the mechanical performance of metals. This paper presents air entrainment measurements for a jet of liquid aluminum alloy A356 plunging into a pool. Measurements are performed in argon and air atmospheres and for a range of jet fall heights. The volume ratio of entrained gas to liquid aluminum poured is measured to be equal to 0.43 for an average jet impact velocity of about 3.8 m/s in the argon atmosphere. This ratio is of a similar magnitude as for water under the same jet parameters. For the corresponding experiment in air, the measured volumetric ratio is only 0.16. It is found that nearly 50 pct of the volume of oxygen entrained is consumed by oxidation, but this alone does not account for the difference between the measurements in inert and oxidizing atmospheres. Instead, the ratio for air is so low because during some portion of the experiment no air was entrained. The onset velocity for gas entrainment for a plunging jet of liquid A356 is found to be 3.9 m/s in an air atmosphere and 3.4 m/s in argon, with the difference attributed to the stabilizing effect of the oxide film on the jet surface in air. These are about three times greater than the onset velocity previously measured for water.

https://doi.org/10.1007/s11663-020-01998-3


## I. INTRODUCTION

AIR entrainment occurs in free surface flows when surface discontinuities entrain air bubbles that are transported into the flow. For many decades air entrainment at the air-water interface of free surface flows has been an important research topic in hydraulics and multiphase fluid mechanics. Two reviews documenting the scope and progress of experimental and computational air entrainment research are presented by Chanson.[1,2] These reviews together provide a valuable perspective of past and recent developments, as they are nearly a decade apart. They document considerable advancement in that time and that air entrainment flows are important in many engineering disciplines and applications. As an example, entrained air reduces the water handling capacity of storm water management and flood control systems, and the systems are designed to minimize air entrainment.[1,2] The experimental work presented here investigates air entrainment in a liquid metal. It contributes not only to the understanding of the casting filling process, but also to understanding other metallurgical processing involving pouring or transferring liquid metal.

Air entrainment occurs at flow disturbances at the free surface and is evidenced by the formation of bubbles. A common air entraining flow during metal casting is the plunging jet shown in Figure 1(a). An example of this flow during casting is the filling of a downsprue. Air entrainment by plunging jet flows have been investigated extensively for water as the fluid medium.[3–11] From the authors' review of the literature, air entrainment measurements have never been performed or published for liquid metals.

As a result of air entrainment during pouring and transfer of liquid metals, oxide inclusions form in ferrous and non-ferrous metals. These inclusions form when liquid metal is exposed to oxygen during mold filling. Oxide inclusions in aluminum alloy castings form as thin solid aluminum oxide films. These inclusions are troublesome as they cannot be removed after the casting process and decrease the performance and life of cast aluminum parts.[12] Air entrainment during mold filling is believed to be a leading source of the oxygen that reacts with the metal to form inclusions.[12,13]

FRANCISCO V. GUERRA, LUCAS ARCHER, RICHARD A. HARDIN, and CHRISTOPH BECKERMANN are with the Department of Mechanical Engineering, University of Iowa, Iowa City, IA 52242. Contact e-mail: becker@engineering.uiowa.edu
Manuscript submitted June 2, 2020; accepted October 2, 2020.
Article published online October 28, 2020.

In this study, a system is developed to measure the volume of gas entrained by a jet of liquid metal plunging into a pool during filling. The gases used are air and argon. Here the pool of liquid metal is formed during filling of a mold cavity since the metal will solidify. Therefore, the part of the measurement system containing the pool is also called a mold. The measurement system is shown in the schematic drawing provided in Figure 1(b) and is described in more detail in the next section of the paper. Experiments are performed using the system to measure air entrainment in water, and agreement between those measurements and results from previous experiments using water verify the accuracy of the measurement system and procedures. Next, twelve experiments are performed using the measurement system in air and argon atmospheres to measure gas entrainment for plunging jet flows using liquid A356 aluminum alloy. These experiments use argon and air atmospheres to compare results for inert and oxidizing gases, respectively. The jet velocity at impact with the pool is an important air entrainment variable[3] and is controlled in these experiments by varying the height of the ladle/nozzle exit above the mold. Measurement results are presented for three heights above the mold using water and the liquid aluminum alloy. For the aluminum alloy experiments, it is found that the collected gas temperature measured during the experiments is required to determine the correct volume of entrained gas. The gas entrainment ratio measured during the experiments, defined as the ratio of volume of entrained gas to volume of liquid poured, is reported and compared for argon and air atmospheres, and water and aluminum liquids. Note in the sections that follow, "air entrainment" is used as a generic term for convenience when describing the gas entrainment measurement system, where air or argon gas atmospheres are used.

## II. EXPERIMENTAL PROCEDURE

### A. *Overview of Air Entrainment Measurement System*

The measurement system used in the current study is shown in the schematic diagram in Figure 1(b). The system was designed based in part on those described in the literature to measure air entrained by plunging water jets. In particular, the studies performed by Wanstall *et al.*[9] and Bates *et al.*[10] were helpful in designing the system, and the system used here follows similar principles. The measurement system uses a reservoir of liquid to provide the jet (or stream of fluid) during the experiment. This reservoir is called a ladle, and a stopper is used to start and end the liquid flow from the ladle. A stable jet of liquid is produced by using a nozzle at the ladle outlet to condition the flow. The volume of fluid in the ladle and the volumetric flow rate are both measured using load cells that record the mass of the ladle during the experiment and the liquid density. The exit velocity from the nozzle can be determined from this data as well. Note in Figure 1(b) that blue lines in the diagram

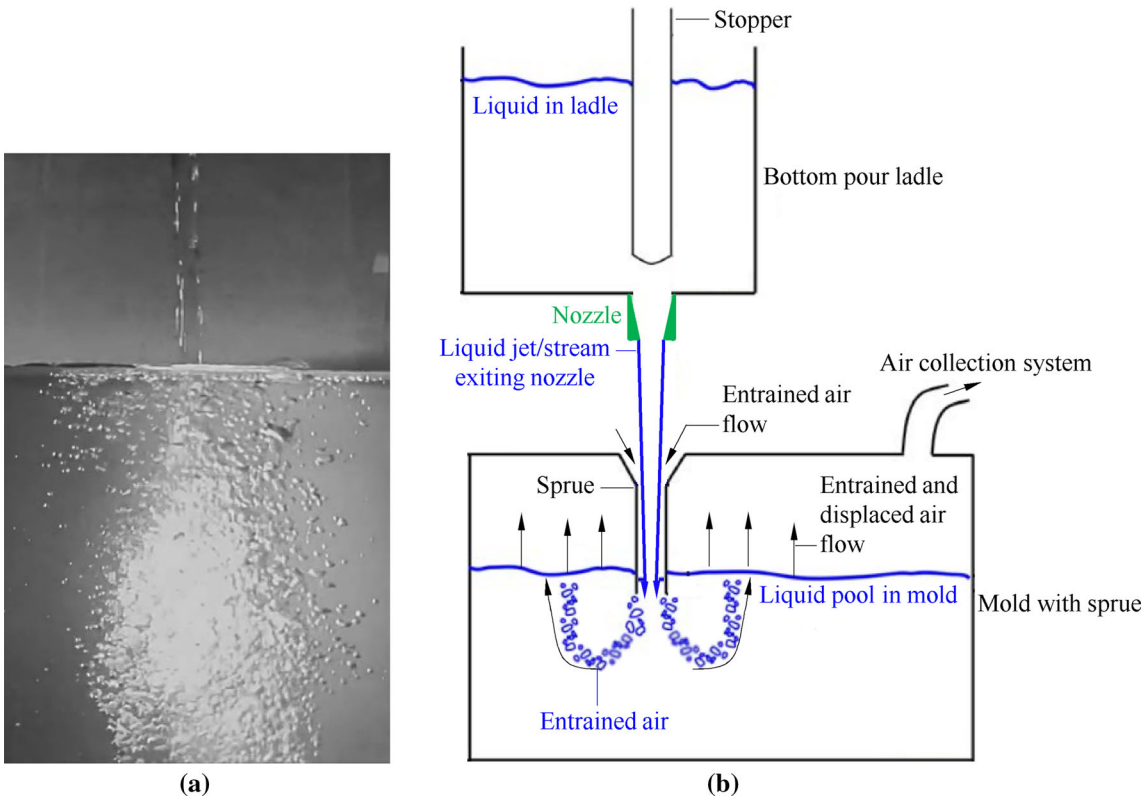


Fig. 1—Air entrainment by a plunging water jet into a quiescent pool. Bubbles (*a*) form at the perimeter of the jet's intersection with the pool. Drawing (*b*) of the air entrainment measurement system with blue lines denoting liquid/gas interfaces.

of the measurement system denote liquid/gas interfaces in the system. As the stream of liquid falls further from the nozzle exit, the velocity of the jet increases and its diameter decreases.

A key component in the current measurement system is a sprue that is built into the top of the mold. The sprue ensures that entrained air is trapped by the fluid stream and cannot escape the sprue once it is entrained. Virtually all entrained air will be transported to the mold cavity and be collected. To prevent entrained air from leaving the measurement system during the experiments, entrained air collection only begins once the sprue is submerged. The sprue diameter is selected so that it is neither too small (and would interfere with the jet of liquid) nor too large (and would not capture the air effectively due to bubble detrainment inside the sprue). Many previous studies of air entrainment for a plunging jet did not use a sprue.[3–8,11]

At the location of the liquid jet impacting the pool, air is entrained at the intersection of the perimeter of the liquid jet and pool once the inertial force of the impinging jet overcomes restraining forces that prevent air entrainment (such as surface tension). The onset of air entrainment also depends upon the turbulence level of the jet, and for low-turbulence water jets the onset of air entrainment occurs at around 1 m/s.[4] As shown by the "Entrained Air Flow" in Figure 1(b), the entrained air is drawn into the sprue and down into the liquid through the space between the jet's stream and the sprue wall. The entrained air is then pulled down into the liquid, and is visible as bubbles. These bubbles then resurface some distance away from the jet impact location. When the sprue exit is submerged, the bulk flow carries the bubbles of entrained air down and out of the sprue where the bubbles then resurface and mix with air above the liquid pool. As shown in Figure 1(b), a mixture of entrained and displaced air flows into a collection bag driven by the pressure created by the volume of entrained air entering the space above the pool, and by the air volume displaced by the rising liquid. After the experiment, the total volume of air collected is measured, and the volume of the air displaced by the liquid filling the mold (the volume of liquid metal poured) is subtracted from it to determine the measured volume of entrained air. Note that the source of the "Entrained Air Flow" in Figure 1(b) is the ambient environment (atmospheric air), or an atmosphere of argon.

### B. *Measurement System Details and Procedures*

The measurement system described in principle in the previous section is described below in practical detail addressing the system's design and procedures used to measure air entrainment for both water and liquid A356. The water measurements were performed to validate the measurements by comparing to previous water studies, and to investigate aspects of the system such as the use of the sprue and effect of elevated liquid temperature on the measurements. A cross-sectional view of the measurement system used is shown in Figure 2(a) with some key dimensions indicated for the bottom pour ladle and mold.

The top end of the measurement system is a bottom pour ladle having a graphite stopper rod to control the liquid flow. The ladle has a capacity of approximately 42 kg of liquid A356. Ceramic fiber blankets were used around the mold to maintain the heat in the ladle between pours. These blankets prevented solidification after pouring and allowed for removal of the lid and sprue after the experiments. This procedure reduced the time between experiments. The ladle is lined with refractory cement in all experiments. The lining is necessary because of the temperatures during the liquid A356 experiments. The nozzle at the ladle outlet is cast from refractory cement as well. The nozzle is designed to condition the flow into a fully-developed profile before the nozzle exit with dimensions given in Figure 2(b). The mass of the ladle is measured from the summed outputs of four load cells. Use of four sensors produces a ladle mass measurement that is insensitive to loading asymmetry. The mass of liquid in the ladle is recorded using data acquisition throughout the experiments, and is reduced to volume, volumetric flow rate and velocity for the liquid jet exiting the nozzle in post-experiment data analysis.

The flow from the bottom pour ladle empties through the nozzle into the pool of liquid filling the mold. The mold is fabricated from 4 mm thick steel lined with refractory cement. A steel sprue with an inner diameter of 4.15 cm is integrated into the lid of the mold and protrudes into the mold so that the sprue exit is 9.37 cm from the bottom of a sprue well. The sprue well reduces the time and volume of liquid required to submerge the exit of the sprue. Before the sprue exit is submerged, it is possible for entrained air to escape up through the sprue, as mentioned in the previous section. Therefore, air collection is delayed until the sprue exit is submerged by liquid. In Figure 2(c) an illustration is given of the entrained air exiting the sprue and as it resurfaces outside of the sprue. It mixes with the air displaced by the pool volume and flows toward the gas collection system. The inlet of the gas collection system is a pipe welded to the top of the mold. The gas is collected and stored in a flexible PVC plastic bag. The collected gas volume is measured after the experiment as described below. Note that air collection is stopped before the ladle empties to avoid the vortex that forms in the ladle when the liquid level is low.

The experimental procedure is described with reference to Figure 3, where a diagram is shown of the measurement system, air/argon collection system and piping network used. Valves used in the experiment are numbered 1 through 6. Three thermocouple (TC) measurements are recorded: in the ladle, at the mold gas exit and at the gas collection bag. Data throughout the experiments is collected from the load cells, TCs and pressure transducers, using a laptop, USB data acquisition hardware, and *DASYLab* software. Before experiments conducted in an argon atmosphere, the mold, collection bag, and piping network are flushed with argon by opening valve 2, and a MiniOX 200 Oxygen Analyzer is used to confirm that the percent of oxygen present in the system is below $0.5 \pm 0.1$ pct. The same analyzer is also used to measure the oxygen content of

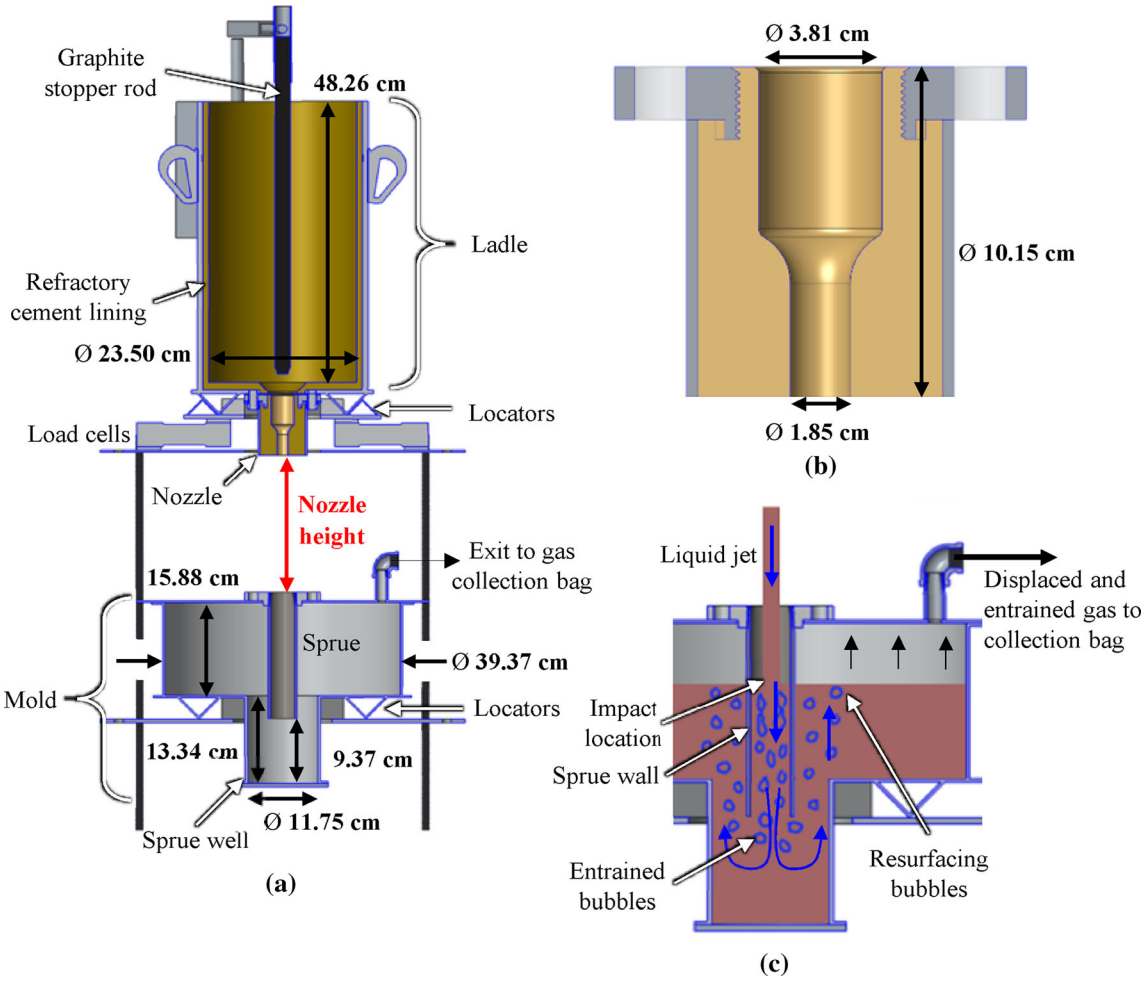


Fig. 2—CAD drawings of the ladle, mold and stand (*a*) used for all experiments. (*b*) Detail view of the nozzle geometry. (*c*) Illustration of air entrainment *via* jet plunging into a mold with a sprue. All drawings are vertical mid-sections.

the collected gas for every experiment. At the start of an air entrainment experiment the lines after valve 1 are cleared using the vacuum pump and valves 2, 3 and 5 are closed. Once the ladle is filled with metal, the three-way valve 1 is turned to the atmosphere. When the stopper is opened the experiment begins, and the stream of metal begins to flow into the mold. After the sprue is submerged by liquid, which can be determined from the load cell readings in real time and takes between 5 to 10 seconds depending on the flow rate of liquid, valve 1 is switched to the gas collection bag. Entrained and displaced gas flows into the collection system during the rest of the experiment until valve 4 is closed and the flow from the ladle is stopped. For the experiments using an argon atmosphere, an argon atmosphere is maintained around the liquid jet using two concentric cylinders that are constantly supplied with argon by opening valve 3, as shown in Figure 3. For the argon experiments the oxygen content of the collected gas was below 0.5 ± 0.1 pct.

After the experiment, the data acquired from the load cells is used to determine the volume and volumetric flow rates of metal poured. The volume of liquid poured into the mold during the experiment, $V_l$, is determined

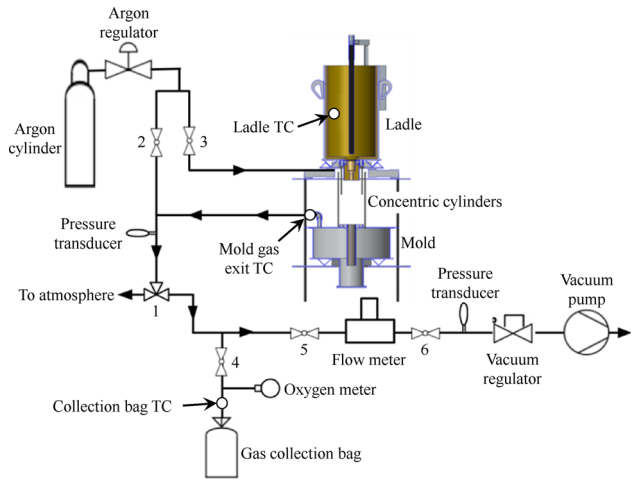


Fig. 3—Diagram of the piping network and gas measurement system used for both the water and aluminum experiments.

from the difference in mass at the beginning and end of air collection and dividing by the density of the liquid poured. For water experiments, a density of 996 kg/m$^3$

was used based on measurement. For the A356 alloy, the temperature in the ladle and temperature dependent density data from thermodynamic software[14] are used to determine the density based on the composition given in Table I. The A356 aluminum alloy has a liquidus temperature of 616 °C.[14] For the A356 experiments the ladle temperature ranged from 627 °C to 768 °C corresponding to a density range from 2425 to 2379 kg/m$^3$. Also, at the conclusion of an experiment, the total volume of air collected, $V_t$, is measured by withdrawing it from the collection bag using a small vacuum pressure (0.99 bar) through a flow meter. An *OMEGA* model FMA1743 flow meter was used. To obtain $V_t$, the measured flow rate is integrated over the duration of withdrawal from the collection bag. The volume of entrained air or argon, $V_e$, is then calculated by

$$V_e = V_t - V_l \quad [1]$$

where $V_l$ is the volume of air displaced by liquid poured into the mold. The entrainment ratio, $V_e/V_l$, is then calculated and provides a result to compare the relative amounts of air entrainment between experiments.

The sensor were calibrated to determine their bias and precision errors. Resulting uncertainties were used to determine measurement errors for the entrained gas volume $V_e$.[15] Average uncertainties for key measured variables and their ranges over all experiments are summarized in Table II. The uncertainty in the temperature correction of the entrained gas was 73 pct on average of the uncertainty in $V_e$ and its largest contributor. This is discussed in the subsection, "Entrained Gas Temperature Correction".

## III. MEASUREMENT SYSTEM TESTING AND VALIDATION USING WATER EXPERIMENTS

The system is first tested using water as the working fluid. Experimental results from these tests are compared to previous work in the literature to validate the measurement system and data reduction procedure. The work by Ervine and Ahmed[5] is often cited and is used here to gage the validity of the measurement system. They found that the air entrainment rate ratio of a low turbulence jet plunging into an open pool of water at room temperature follows the correlation

**Table I. A356 Aluminum Alloy Composition (Wt Pct)**

| Alloy | Si | Mg | Fe | Ti | Zn | Cu | Mn |
|---|---|---|---|---|---|---|---|
| A356 | 7.00 | 0.37 | 0.10 | 0.08 | 0.01 | 0.01 | 0.01 |

$$\frac{Q_e}{Q_l} = 0.003\,\frac{u_j^2}{g d_j} \quad [2]$$

where $u_j$ is the jet velocity at impact, $g$ is the acceleration due to gravity, and $d_j$ is the jet diameter at impact. The correlation indicates that entrainment should increase both for increasing $u_j$ and decreasing $d_j$. The variables in the correlation form the Froude number squared for a plunging jet, where the Froude number is defined as[5]

$$Fr_j = \sqrt{\frac{u_j^2}{g d_j}} \quad [3]$$

The Froude number gives the ratio of inertial to gravitational forces for a plunging jet.

Filling simulations are performed[16] to investigate the effect of the sprue on the variables $u_j$ and $d_j$, and the measured air entrainment. In these simulations of the air entrainment measurement system, the measured flow rates from the water experiments are used in the filling simulations. Simulation results were compared for cases with and without using a sprue. Cross sectional views of the absolute velocity field during filling of the measurement system is shown for both cases in Figure 4. The images in Figure 4 coincide with the midway point during the gas collection process. The most significant effect of the sprue is to cause a depression of the impact location of the jet relative to the free surface of the liquid pool surrounding the sprue. This is shown in Figure 4(a) and is compared to the case without a sprue shown in Figure 4(b). Because of this depression of the metal surface inside the sprue, the liquid metal falling height from the nozzle outlet is greater with the sprue. A lower impact location (or increased falling height) increases the jet velocity at impact, $u_j$, and also decreases the jet diameter at impact, $d_j$. Considering these effects and the correlation Eq. [2], the use of a sprue in the measurement system should increase the entrainment rate over not using a sprue for the same experimental conditions (*i.e.* flow rates and nozzle height from the mold inlet).

As a consequence of using the sprue in the measurement system (as discussed relative to Figure 4), there is a depression of the liquid level in the sprue and a corresponding increase in the metal falling height compared to not using the sprue. Because of the amount of this depression, which is predicted by filling simulations to vary marginally, the parameters of the impinging jet (falling height and velocity) are not calculable from the experimental conditions alone. The best method ascertained by the authors to determine the actual falling height during the experiments was to determine them from filling simulation results for each experiment using measurement of the flow rate, the nozzle exit diameter and nozzle height. This method was verified using video recordings of the experiments with water. Over the duration of an experiment, from start to end of gas collection, the jet velocity and falling height are determined along with their variations. The falling height was determined during the experiments based on the average position of the liquid free surface in the

sprue from the simulations. The range of falling heights for a given experiment is taken as the minimum to maximum values as discussed below.

The jet parameters are determined from the experimental data and the filling simulations. The falling height, $h_j$, is determined first from the simulation results as described above. From the falling height and the nozzle exit velocity, $u_N$, (determined from the measured flow rate), the jet velocity, $u_j$, at impact is calculated during gas collection period using

$$u_j = \sqrt{u_N^2 + 2gh_j} \quad [4]$$

The jet diameter, $d_j$, at impact is therefore

$$d_j = d_N \sqrt{\frac{u_N}{u_j}} \quad [5]$$

where $d_N$ is the diameter of the nozzle exit. The jet parameters are then used in analysis of the experiment results and in comparisons with the correlation given by Eq. [2].

In Figure 5 entrainment results using water are summarized and compared to the correlation. In Figure 5(a) air entrainment ratio, $V_e/V_l$, results using the measurement system with the sprue and a 33 cm nozzle height are compared to Eq. [2] with and without using a sprue. The experimental result is the average of two experiments using the sprue, and the bar is the range of the results. For the correlation cases, the flow rate measured during the water experiments and the nozzle diameter are used to calculate $u_j$ and $d_j$ at each time step of recorded data during the experiment. Then at each recorded time step Eq. [2] is used to calculate $Q_e/Q_l$, which is integrated over the time that air is collected during the experiment to obtain $V_e/V_l$ for the correlation cases plotted in Figure 5(a). Results in Figure 5(a) demonstrate the experimental results agree well with the correlation for the sprue, and that the additional falling height resulting from the sprue needs to be considered in analyzing the measurements. Considering the correlation results in Figure 5(a), the air entrainment ratio increases by close to 50 pct when a sprue is used for the 33 cm nozzle height.

Since the aluminum experiments are performed in both air and argon atmospheres, water experiments were conducted in both air and argon atmospheres as well for three nozzle heights as shown in Figure 5(b). In the figure the average measured entrainment ratios from two experiments at each height and atmosphere are given. The bars in the figure are the ranges of values from the two replicated experiments. From Figure 5(b) it is found that a plunging jet entrains the same volume of argon and air in the measurement system at each nozzle height. This finding demonstrates that any difference in air entrainment experimental results between argon and air atmospheres when pouring liquid aluminum is not due to the atmosphere used, or the measurement system and procedures.

In Figure 5(c), the measured air entrainment ratios from the water experiments and the plunging jet correlation Eq. [2] are plotted against Froude number. In this figure, horizontal bars on Froude number scale are the range of Froude numbers during the experiment from the start of air collection (the upper value) to the end of collection (the lower value). Vertical bars in the figure are the range of entrainment ratios from two experiments performed under the same conditions. The symbols are located at the average entrainment ratio, and Froude number measurements. An impact jet diameter of $d_j$ = 1.49 cm is used in plotting the water plunging jet correlation Eq. [2] as it is the overall average diameter for the measurements. The measured air entrainment ratios are in reasonable agreement with the correlation Eq. [2] proposed by Ervine and Ahmed[5] for water. The best agreement between measurement and correlation is seen in the 33 cm nozzle height experiments. The best correspondence between correlation and measurement is at the lower end of the Froude number ranges, which occur near the end of the gas collection. Considering these results, the measurement system and approach has good validity for investigating the influence of the jet parameters on air entrainment in liquids, including liquid A356.

### A. *Entrained Gas Temperature Correction*

Considering the effects of temperature on the measurements, the volume of entrained air is independent of the air temperature, but the same cannot be said for the liquid temperature. As succinctly stated by Chanson,[1] "air bubbles may be entrained when the turbulent kinetic energy is large enough to overcome both surface tension and gravity effects." Clearly the liquid surface tension is a function of temperature is therefore important both to the onset (affecting the critical velocity) and amount of air entrainment. Here however, experimental results are compared with the correlation given by Eq. [2] which was developed for water at room temperature and is not dependent on surface tension. As a result, liquid temperature-surface tension effects are not considered in the experimental data reduction. For the current work, it is foremost to consider the effects of temperature on the entrained gas volume measurement and its data reduction procedure. The total volume of air displaced and entrained is measured at room temperature following the experiment, but the displacement and entrainment occur at an elevated temperature during the experiments. Therefore, it is necessary to correct the measured volume of gas entrained and displaced, $V_t$, to account for the difference between the measured gas temperature (room temperature) and the entrained gas temperature.

To determine a procedure for the measurement of the entrained air volume at different temperatures, Eq. [2] is used with along with air entrainment experiments performed using water at room temperature and at a higher temperature for the same jet velocity and diameter. Assuming surface tension effects are negligible for the two cases, the volume entrained in these two experiments should be equal once the correct air entrainment temperature is used to determine its volume for the higher temperature water experiment. For the higher temperature case, experiments using hot water

Table II. Averages and Ranges of Uncertainties Over All Experiments for Key Measurements

| Measured Variable | Average Uncertainty for All Experiments | Uncertainty Range for All Experiments |
|---|---|---|
| Mass of A356 | 0.03 kg | — |
| Volume of A356 $V_l$ | 0.25 pct | 0.19 pct to 0.32 pct |
| Gas Volume Collected $V_t$ | 1.76 pct | — |
| Volume of Gas Entrained $V_e$ | 4.4 pct of $V_t$ | 3.9 to 5.9 pct of $V_t$ |

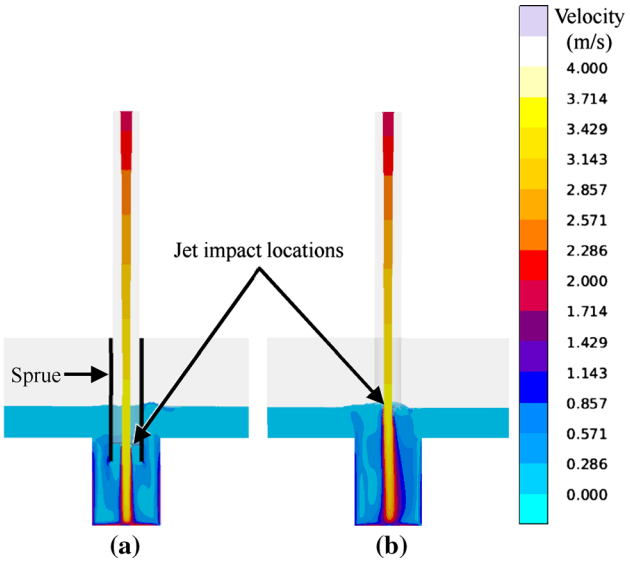


Fig. 4—Velocity contours from water filling simulations comparing the jet impact locations (*a*) with a sprue (in black) and (*b*) without a sprue, midway through gas collection.

(80 °C) were conducted to investigate the effect of the temperature change on the volume of gas entrained and displaced. The difference between the volumes of entrainment measured in these hot water experiments and measurements at room temperature (23 °C) were compared. A method of determining the best approach to correct the air volume for the hot water experiments was determined so that the corrected volume was equal to the room temperature volume of entrained air. Then, this correction method was applied to the experiments performed when pouring A356.

The leftmost bar in Figure 6 gives the relative volume of air entrained for two experiments using 80 °C water conducted using a 33 cm nozzle height. The range of the two experiments is given by the bars, and without using the correct entrained air temperature the relative air entrainment ratio is about 0.2. The rightmost bar shows the 23 °C result at about 0.32, where the bars indicate the range for two experiments. The difference between the experiments conducted with 80 °C and 23 °C water is about 38 pct and demonstrates that it is necessary to correct the entrained air volume for the higher temperature case.

To correct the entrained volume measurement, the temperatures of the entrained and displaced gas are needed. Unfortunately, measurements of the temperatures of the entrained or displaced gas are impractical. As a first approximation, it is reasonable to assume that the temperature of the entrained and displaced gases is equal to the temperature of the gas exiting the mold, which is readily measurable. During the 80 °C water experiments, the temperature of the collected gas exiting the mold remained relatively constant throughout each experiment at 50 °C. This steady value of the temperature of the gas exiting the mold, $T_{ex}$, was used to correct the total volume of gas collected during the experiment, $V_t$, measured at the ambient temperature, $T_{amb}$, based on the ideal gas law using

$$V_{t,\text{corr}} = V_t \frac{T_{ex}}{T_{amb}} \quad [6]$$

where $V_{t,\text{corr}}$ is the corrected total volume of gas collected. Since Eq. [6] is based on the ideal gas law, absolute temperatures are used. The temperature-corrected entrained gas volume, $V_{e,\text{corr}}$, is then found using Eq. [1] by subtracting $V_l$ from $V_{t,\text{corr}}$. The temperature-corrected gas entrainment ratio is therefore $V_{e,\text{corr}}/V_l$.

When the entrainment ratios for the 80 °C water experiments are corrected for temperature using this method, they are in good agreement with the air entrainment results from the 23 °C water experiment as shown in Figure 6. Following testing and validation of the measurement system and procedures using entrainment experiments with water, the system was used to perform experiments using the A356 aluminum alloy as presented below.

## IV. RESULTS AND DISCUSSION

### A. *Measurements and Experimental Results*

Air entrainment experiments for liquid A356 were performed at nozzle heights of 13, 23 and 33 cm, and at each nozzle height experiments were run in argon and air environments. These height and gas conditions combine to produce six experimental cases. Each experimental case was repeated once so that twelve aluminum air entrainment experiments were carried out in this study.

During each air entrainment experiment the volume of liquid aluminum in the ladle, the temperature of the aluminum in the ladle, the mold gas exit temperature and the temperature of the gas in the collection bag were recorded. In Figures 7(a) and (b) the measured volume and temperature data for all experiments are plotted *vs* time using line colors to identify the experimental cases

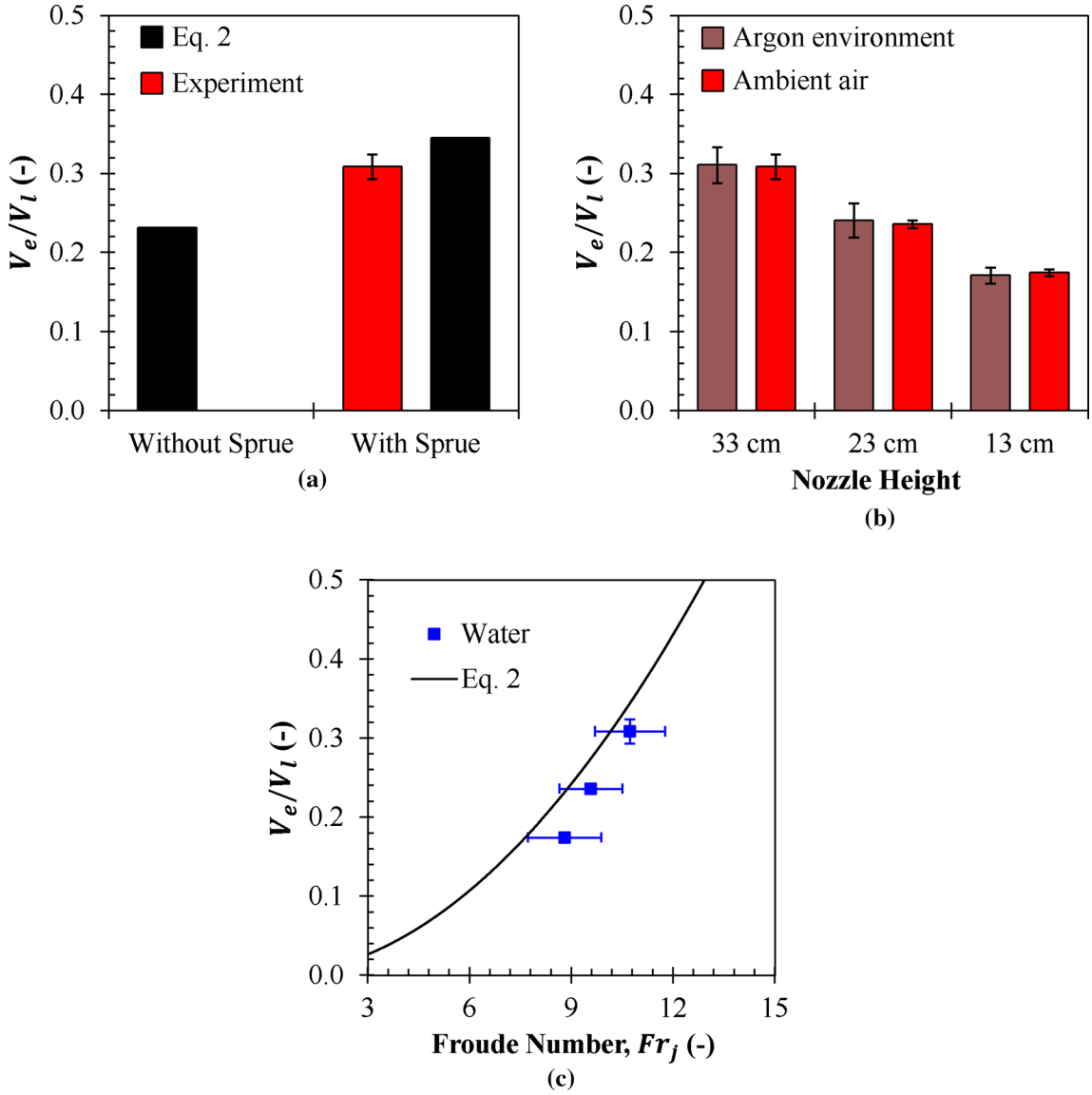


Fig. 5—Entrainment measurements using water. (*a*) Air entrainment ratio with and without a sprue from correlation Eq. [2] and experiment with sprue. (*b*) Entrainment ratio results for three nozzle heights using air and argon atmospheres. Bars are the range of two experiments. (*c*) Measured entrainment ratio and correlation Eq. [2] plotted against Froude number. Vertical bars are the range from two experiments. Horizontal bars are the *Fr* range during the experiments.

corresponding to the bar colors and atmosphere-nozzle height cases labeled in Figure 7(c). The time axes in Figures 7(a) and (b) begin at 10 seconds before the start of filling. The starting and ending times of gas collection are indicated in Figures 7(a) and (b). Flow rates during the experiments were calculated using the slopes of the curves in Figure 7(a) calculated at one second intervals, and these were relatively consistent. Temperature measurements during the experiments are shown in Figure 7(b). In this figure the A356 temperature measurements in the ladle increase after it is filled before pouring the experiments. The temperature increase is due to the ladle and sensor heating up and the sensor response. Considering this, the upper plateau of these curves is taken to be the pouring temperature. The pouring temperature of the liquid aluminum in the ladle ranged from 625 °C to 770 °C during the experiments. The temperature of the gas in the collection bag was essentially constant for all experiments and was equal to the ambient temperature, 27 °C. The temperature of the gas exiting the mold, $T_{ex}$, increases with time as the mold gas heats and the sensor responds. From midway through the gas collection time interval and until 6 seconds after the end of collection, the mold gas exit temperatures plateau to nearly steady values for each experiment. The mold gas exit temperatures for the experiments are taken as the time averages of each of these plateaus, and ranged from approximately 70 °C to 120 °C. The time interval used for the averaging is 12 seconds and roughly equal to gas collection time.

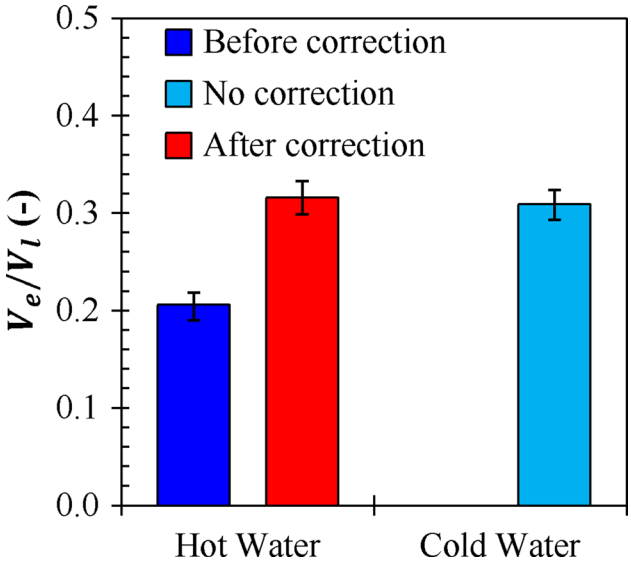


Fig. 6—Entrainment ratio results from water experiments comparing hot water experiment entrainment ratios before and after temperature correction with the cold water entrainment ratio. Bars are the range of two experiments.

In Figure 7(c) the volumes of aluminum poured during gas collection are directly compared to the volumes of gas measured in the collection bag after the experiments at room temperature. In all experiments except the two poured in argon environment at 33 cm nozzle height, the total volume of gas collected, $V_t$, is less than the volume of aluminum poured, $V_l$. This is physically impossible as the volume of gas collected must at least equal the mold volume filled during pouring. This observation demonstrates that the volume of collected gas measured at room temperature must be corrected to account for the actual entrained gas temperature during the measurement process.

The falling heights and jet parameters determined from the filling simulations and experimental data for A356 are given in Figure 7. In this figure the line colors correspond to the colors for the cases labeled on the horizontal axis of Figure 7(c). In Figure 8, the origins on the time axes are the start of pouring, and data is only shown during the entrained gas collection time interval, which are slightly different among the experiments. Note the difference in the time scale when comparing to the time axes in Figures 7(a) and (b), which begin 10 seconds before the start of filling. The falling height, $h_j$, determined from simulation results is shown in Figure 8(a). The jet velocity, $u_j$, at impact is calculated during gas collection period from Eq. [4] and is plotted in Figure 8(b). The jet diameter, $d_j$, results calculated from Eq. [5] are plotted in Figure 8(c). In Figure 8(d), the Froude number from Eq. [3] is plotted over the gas collection period for all experiments.

In Figure 8(a), the data fall into three groups corresponding to the three nozzle heights with larger heights corresponding to larger velocities. The jet parameters are somewhat grouped as well with nozzle height in Figures 8(b), (c) and (d), but not as tightly. The parameters in these figures are less tightly grouped particularly for the cases with lower nozzle heights (23 and 13 cm) due to differences and variations in flow rates and the nozzle exit velocities. Over the experiment duration, the falling height decreases as the mold is filled and the liquid level rises. In Figure 8(a), the largest falling heights correspond to the tallest nozzle heights. The velocity of the jet at impact in Figure 8(b) follows the same trend as the falling height. The jet diameters in Figure 8(c) decrease throughout each experiment as well. Looking at the 33 cm nozzle height case, the jet velocities vary by about 14 pct during the experiment and the jet diameter has about half that variation. Less variation in the jet diameter is due the counter acting effects of the liquid level rising (which would increase the jet diameter during the experiment for a constant nozzle velocity) and the decrease in nozzle velocity over the experiment duration. The Froude number shown in Figure 8(d) is a key parameter in air entrainment correlations from previous studies, including the correlation given by Eq. [2]. The Froude number appears to show more variability between experiments with smaller falling heights as well. Again, based on the 33 cm nozzle height cases, the Froude number varies by about 11 pct over the experiment duration (from 11 to 9.8).

To summarize the experimental jet parameter results for a combination of atmospheric and falling height conditions, representative values of the parameters and their variation are defined for each experimental case. The value used to represent the jet parameters for each experiment is the average of the data over the experiment duration shown in Figure 8. The value used to represent the variation of jet parameters for an experiment is the data range for each experiment, the difference between the maximum and minimum values plotted in Figure 8. Note that four experiments were conducted at each nozzle height as shown in Figure 7(c), two in an argon atmosphere and two in an ambient air atmosphere. Since two experiments were performed for each measurement condition (nozzle height and gas entrained), the jet parameter result reported here for each experimental condition is the average of the two average values from the two experiments performed for each condition. Similarly, the variation of the jet parameter result reported here is the average of the two ranges of data from the two experiments performed for each experimental case. The results of the jet parameters and their variations for all experimental cases are given Table III, organized by atmosphere and nozzle height used. The average jet velocity, $\bar{u}_j$, and Froude number, $\overline{Fr}_j$, all decrease with lower nozzle heights. The average jet diameter at impact, $\bar{d}_j$, increases with lower nozzle heights. These results are in accordance with the fundamental physics for a jet of liquid plunging into a pool. The measured entrainment ratio, $V_e/V_l$, from the experiments in liquid A356 is presented next, and is followed later by discussion of the relationships between the jet parameters in Table III and measured air entrainment.

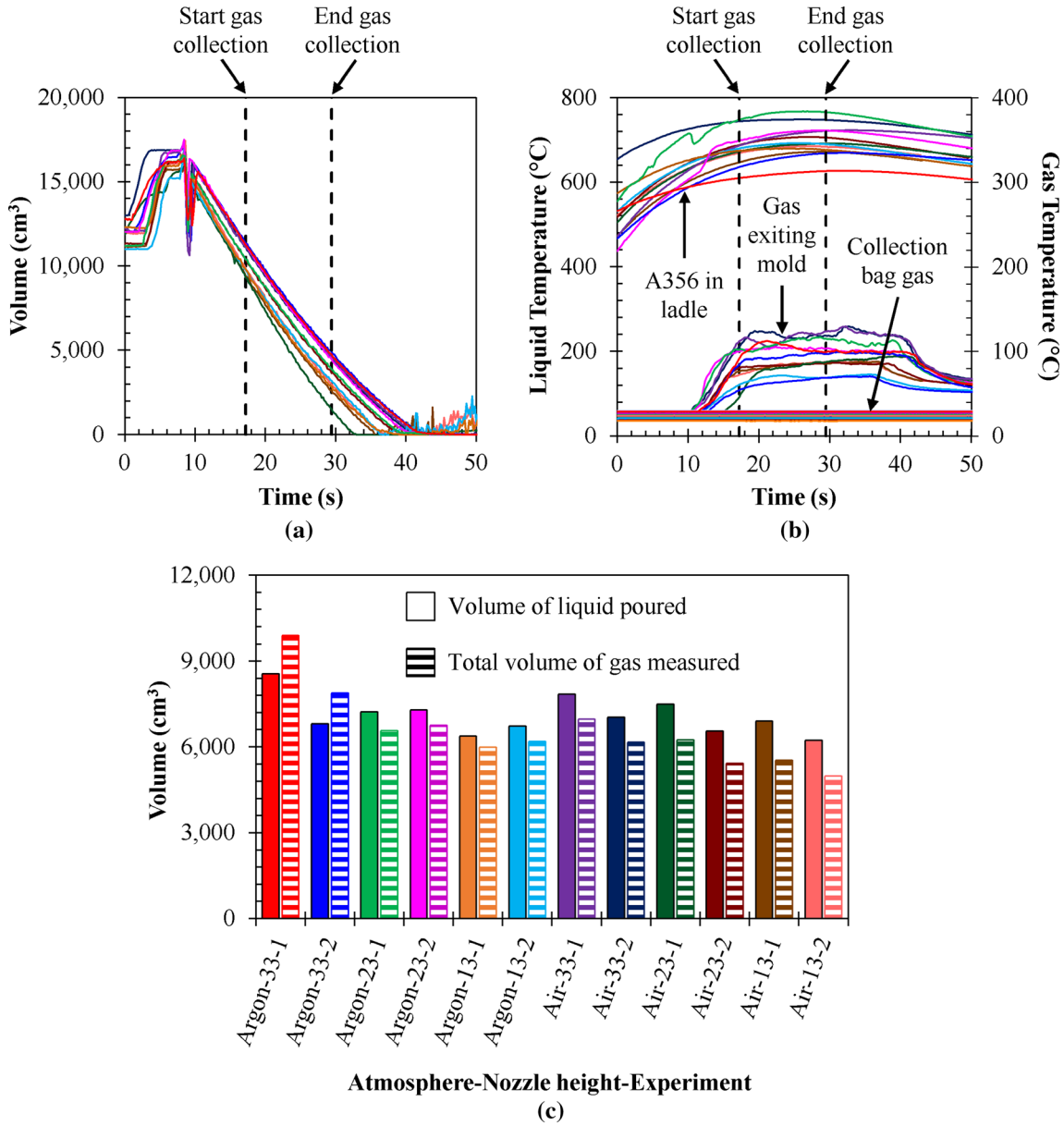


Fig. 7—Measurements during aluminum experiments: (*a*) volume of aluminum in the ladle and (*b*) temperatures of aluminum in the ladle, gas exiting the mold and in the collection bag. Measurements determined after the experiments: (*c*) volume of aluminum poured during air collection, and total collected gas volume measured at room temperature. The line color legend for the twelve experimental cases is given by (c) (Color figure online).

The temperature-corrected gas entrainment ratios measured for the experimental cases are shown in Figure 9. The results plotted in Figure 9 are the average values and ranges from the two experiments performed for a combination of atmospheric and falling height conditions. The vertical bars indicate the range of values from the two experiments, and these show good reproducibility.

For A356, the gas atmosphere (inert argon or air) has a large effect on air entrainment. For example, the entrainment ratios for the experiments conducted with a 33 cm nozzle height are 0.43 in an argon atmosphere and 0.16 in air, as shown by the two leftmost bars in Figure 9. For the water experiments, the type of gas did not affect the entrainment ratio. In Figure 9, the entrainment ratio for the A356-argon experiments decreases from 0.43 to 0.16 when the nozzle height is lowered from 33 to 23 cm, and decreases from 0.16 to 0.08 when the nozzle height is lowered from 23 to 13 cm. This corresponds to a 63 pct decrease from 33 to 23 cm, and 50 pct from 23 to 13 cm. For the experiments discussed earlier using water and similar flow rates, the commensurate decrease was only 22 pct from 33 to 23 cm, and 29 pct from 23 to 13 cm (Figure 5(b)).

### 1. *Analysis of $O_2$ consumption to form oxides and effect on measured air entrainment*

The difference between the measured gas entrainment for the two gas environments could result from entrained oxygen being consumed to form oxide films in air. Less gas would be collected during air

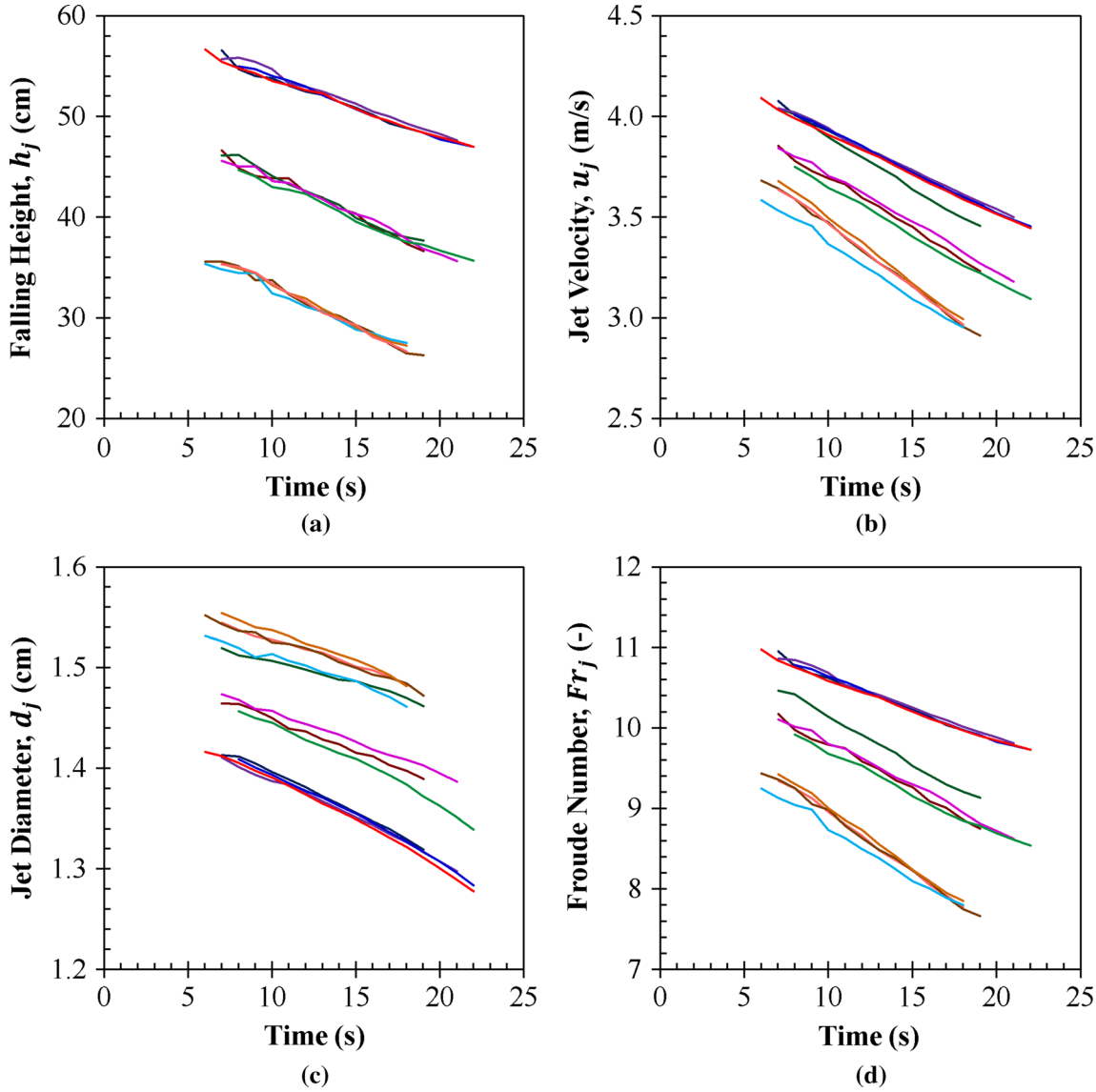


Fig. 8—Jet parameters *vs* time during gas collection for A356 experiments with nozzle heights of 33, 23 and 13 cm. (*a*) Falling height determined from filling simulations, decreasing during filling. Other jet parameters are calculated in sequence: (*b*) jet velocities, (*c*) jet diameters, and then (*d*) Froude numbers. Line color legend in Figure 7(c) (Color figure online).

**Table III. Experimental Conditions and Their Jet Parameters and Variations for A356 Experiments**

| Atmosphere | Nozzle Height (cm) | Average Jet Velocity, $\bar{u}_j$ (m/s) | Average Jet Diameter, $\bar{d}_j$ (cm) | Average Froude Number, $\overline{Fr}_j$ (—) |
|---|---|---|---|---|
| Argon | 33 | 3.76 ± 0.28 | 1.36 ± 0.06 | 10.30 ± 0.55 |
| Air | 33 | 3.78 ± 0.26 | 1.36 ± 0.05 | 10.34 ± 0.52 |
| Argon | 23 | 3.47 ± 0.31 | 1.42 ± 0.05 | 9.29 ± 0.67 |
| Air | 23 | 3.65 ± 0.30 | 1.46 ± 0.03 | 9.63 ± 0.69 |
| Argon | 13 | 3.32 ± 0.32 | 1.51 ± 0.03 | 8.61 ± 0.73 |
| Air | 13 | 3.31 ± 0.34 | 1.51 ± 0.03 | 8.58 ± 0.79 |

Values are the average of the two average values from the experiments performed for each case. Ranges are average of the two ranges from the experiments performed for each case.

experiments compared to those in argon atmosphere under the same conditions. To investigate the reduction in the measured entrained air volume due to oxygen consumption, results from the 33 cm nozzle height experiments with air atmosphere were used to perform exploratory calculations. For this height the average oxygen level was reduced by 1.35 pct. The average air entrainment volume was found to be 1223 $cm^3$. The

volume of $O_2$ consumed to form oxides can be calculated assuming that no nitrogen is consumed to form nitrides, and the air is comprised of $O_2$ and $N_2$ only. Under these assumptions the volume of $N_2$ entrained is 1079 $cm^3$. The volume of air entrained that would have been collected if no $O_2$ was consumed is 1366 $cm^3$. The volume of entrained oxygen that would have been collected if no oxygen was consumed is therefore 287 $cm^3$. However, the volume of entrained oxygen collected was actually (1223 to 1079) $cm^3$ or 144 $cm^3$. Therefore, the volume percentage of entrained oxygen consumed was ((287 to 144)/287) or 49.8 pct. Since only about half of the entrained oxygen was consumed, oxide films are likely shielding the aluminum from further oxidation.

For the ambient air experiments with a 33 cm nozzle height the measured air entrainment ratio was (1223 $cm^3$)/(7444 $cm^3$) = 0.16. If no oxygen were consumed, the entrainment ratio would have been (1366 $cm^3$)/(7444 $cm^3$) = 0.18, an increase of only 0.02. The air entrainment ratio without oxygen consumption is still less than half of the air entrainment ratio measured for experiments conducted in an argon atmosphere at the same nozzle height, 0.43 as shown in Figure 9. Clearly a cause other than entrained oxygen consumption is responsible for the reduced air entrainment measurement in the air atmosphere. It is believed that the substantial difference between the measured entrainment ratios for argon and air results from the solid oxide film forming on the jet surface. This film would act to reduce the surface turbulence of the jet and this would decrease the volume of gas entrained.

To demonstrate the significance of oxide film formation in A356, the measurement and analysis of the oxygen reduction can be used to calculate the mass and surface area of aluminum oxide films that forms due to air entrainment. Using molar analysis when 49.8 pct of the oxygen in the entrained air is consumed, a mass fraction of 16.1 ppm aluminum oxide ($Al_2O_3$) in the aluminum alloy poured is obtained. It is relevant to note that $Al_2O_3$ forms as a thin layer, only 4 nm thick [17]. Considering such a thin oxide layer, this equates to an $Al_2O_3$ sheet area of 27.8 $m^2$ when 18.6 kg of A356 is poured.

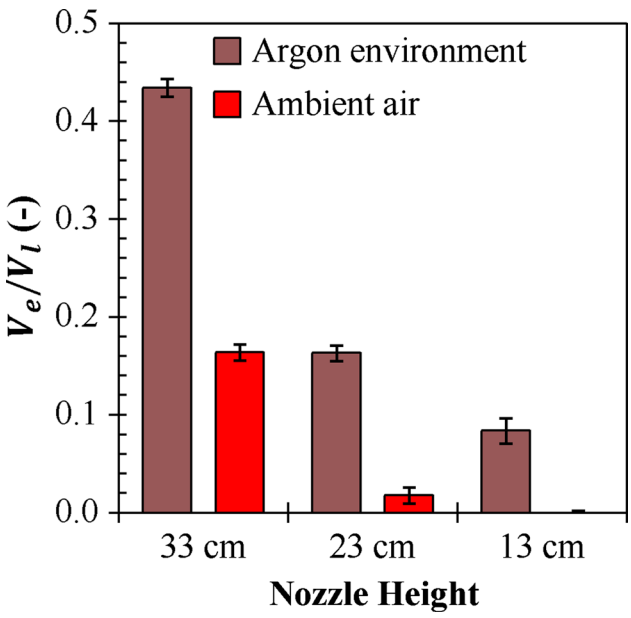


Fig. 9—Temperature-corrected entrainment ratios from aluminum experiments. Vertical bars indicate the range of values from two experiments.

### B. *Discussion of Air Entrainment Results*

The entrainment ratios from the aluminum experiments are plotted against the jet impact velocity in Figure 10(a) and Froude number in Figure 10(b). The water plunging jet correlation Eq. [2] is also plotted in both Figures 10(a) and (b). An impact jet diameter of $d_j$ = 1.44 cm (the average for all experiments) is used in plotting Eq. [2]. Vertical bars in Figure 10 on the average measurements are the range of entrainment ratios measured from two experiments performed under the same conditions. The horizontal bars in Figure 10 on the average velocity and Froude number measurements give the range (maximum and minimum) of the values over the duration of the experiments performed for the same conditions. The maximum velocities in these results occur at the start of the experiment's gas collection process.

The measured air entrainment ratio for the aluminum experiments performed using both argon and ambient air environments are found to have a quite different dependency on the measured jet parameters than the water experiment data and correlation. The volume of air entrained by a plunging jet of the aluminum alloy, in both atmospheres, appears to be more sensitive to changes in the jet impact velocity, $u_j$, than the volume of air entrained by a plunging jet of water, as seen in Figure 10(a) by the steep increase in entrainment with increasing velocity. A similar trend is observed in Figure 10(b) when the entrainment ratios are plotted against the Froude number. In Figure 10, the lowest air entrainment results correspond to the 13 cm nozzle height, the next higher values correspond to the 23 cm cases, and the highest air entrainment was measured in the 33 cm nozzle height experiments. The entrainment ratio for the A356-argon experiments at the 33 cm nozzle height is above the line representing the correlation for water, while all other A356 measurements fall well below the line. The low or vanishing entrainment ratios in Figure 10, and their subsequent steep increase, can be explained by the jet not overcoming the critical conditions necessary for entrainment to commence, which is discussed in detail in the following paragraphs. The relatively high value for the A356-argon experiments at the 33 cm nozzle height indicates that once entrainment does begin, the amount of gas entrained for A356 is as large as or larger than that for water.

As mentioned in Section II–A, gas entrainment commences once the inertial force of the impinging jet overcomes restraining forces that prevent air entrainment. The onset of air entrainment, termed the inception point, also depends upon the turbulence level of the jet. Based on the ranges of jet velocities in Figure 10,

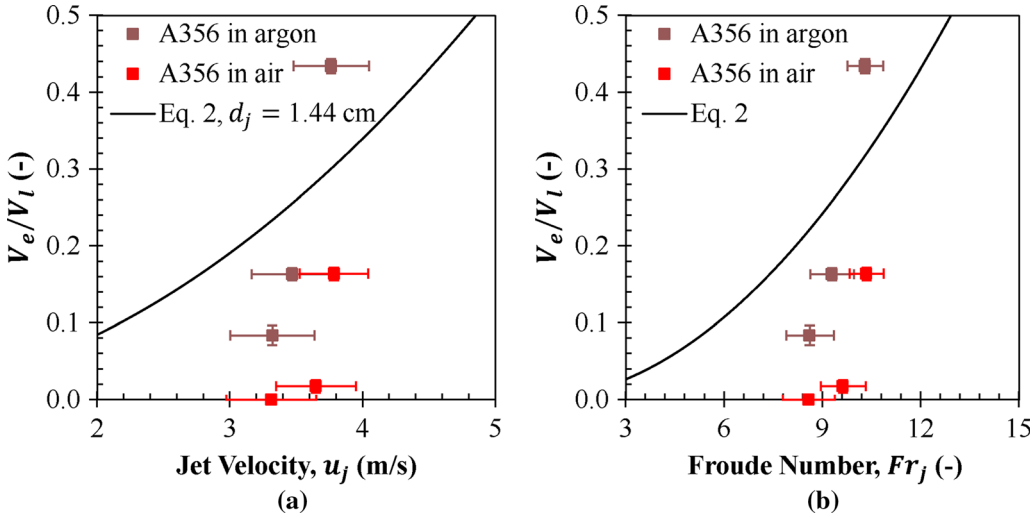


Fig. 10—Temperature-corrected entrainment ratios from aluminum alloy experiments and the water plunging jet correlation Eq. [2] plotted against (*a*) jet velocities, and (*b*) Froude number. Vertical bars are the range of entrainment ratios from two experiments. Horizontal bars give the range of the values over the duration of the experiments. An impact jet diameter of $d_j$ = 1.44 cm is used in plotting the correlation Eq. [2].

estimations of the critical velocity, $u_e$, and inception point for A356 in air and argon atmosphere can be made. For the A356-air experiments, no air entrainment was measured with the 13 cm nozzle height and according to Table III the impact jet velocities ranged from 2.97 to 3.65 m/s. Hence, the critical jet velocity must be above about 3.7 m/s. Considering the 23 cm nozzle height experiments for A356-air, the impact jet velocities ranged from 3.35 to 3.95 m/s and the air entrainment ratio measured was slightly above zero at 0.02. This indicates that air was entrained only at the very beginning of the 23 cm experiments and the critical velocity is only slightly below 3.95 m/s. Based on these observations, a reasonable estimate for the critical velocity, $u_e$, for A356-air is 3.9 m/s, but it could be as low as 3.7 m/s. For the 33 cm nozzle height case with A356-air the measured air entrainment ratio was somewhat higher, at 0.16, and the jet velocities ranged from 3.52 to 4.04 m/s (Table III). If the critical velocity is indeed about 3.9 m/s, then even for the 33 cm case no air was being entrained over a significant portion of the experiments. This explains why the measured entrainment ratio of 0.16 for this case is still far below the line from the correlation for water (Figure 10).

Since significant entrainment was measured in the A356-argon experiments for all nozzle heights, determining the inception point and critical velocity is more difficult and requires extrapolating the results. For the 13 cm nozzle height, the impact jet velocities ranged from 3.00 to 3.64 m/s for the A356-argon experiments (Table III), and the entrainment ratio measured was 0.08. While this shortest nozzle height produced some entrainment, it was likely not entraining argon for the entire experiment duration. This means the critical velocity is greater than 3 m/s and less than 3.6 m/s. For the highest fall height argon experiments, the air entrainment ratio is 0.43 and is the largest measured over all experiments. The steep increase in air entrainment over the 13 cm nozzle height case is only likely to occur if entrainment is occurring throughout the entire 33 cm experiments. Jet velocities for the 33 cm case range from 3.48 to 4.04 m/s. This indicates that the critical velocity is less than 3.5 m/s. Next considering the 23 cm nozzle height experiments in argon, the jet velocities ranged from 3.16 to 3.78 m/s. The entrainment ratio measured was 0.16, which is twice the amount measured for the 13 cm height. However, the amount of air entrained and the increase over the 13 cm case do not indicate air was being entrained throughout the entire experiment. So the critical velocity must be greater than 3.2 m/s. Considering this and the twofold increase in the entrainment ratio between the 13 and 23 cm cases, a reasonable estimate for the critical velocity for A356-argon is 3.4 m/s, with a lower bound of 3.2 m/s. Then, argon would be entrained from 3.4 to 3.6 m/s during the 13 cm case and between 3.4 and 3.8 m/s for the 23 cm case (and during the entire 33 cm case).

Comparing Figures 5 and 10, the differences in entrainment ratios and sensitivity in changes to nozzle heights between the water and aluminum experiments are not due to flow rates and volumes poured, since these were similar. The differences could be explained by the fluid properties. Table IV reports important fluid properties for both water and A356 aluminum alloy. The density of water was measured. The sources for the other fluid properties are shown in Table IV. The surface tension of water is more than ten times lower than the surface tension of A356. This might explain the difference between the measured entrainment ratios for the same changes in falling heights for the water and aluminum experiments performed under similar conditions.

The critical velocities estimated above for the A356 experiments are found to be significantly higher than 1 m/s, an often cited value for the inception velocity for water,[4] but the inception velocity depends upon variables such as turbulence intensity and jet diameter, among others. The order of magnitude difference

between water and A356 surface tension is one possible explanation for the difference in critical velocities. Ciborowski and Bin[11] give a critical jet Weber number, $We_j$, for the inception point and a correlation for the critical jet velocity, $u_e$, which includes the effects of surface tension as

$$We_j = 400 \text{ or } u_e = \sqrt{400 \frac{\sigma}{\rho d_j}} \quad [7]$$

Using Eq. [7], the fluid properties of water and liquid A356 from Table IV, and the average jet diameters from the water and A356 experiments (1.49 and 1.44 cm, respectively) the $u_e$ is 1.40 m/s for water and 3.21 m/s for A356. The results from Eq. [7] agree well with the finding of this study (1) that the inception velocity for A356 is much higher than for water, and (2) that the inception velocity for the present A356-argon experiments is at least 3.2 m/s. Surface tension effects are indeed important when comparing the experimental results for water and A356, but according to Eq. [7] the more than two-fold difference in density plays a role as well. The fact that the estimated critical velocity for the A356-air experiments (3.9 m/s) is significantly higher than for the A356-argon experiments (3.4 m/s) could be explained by the stabilizing effect of the oxide film that is covering the jet in the air experiments. Due to residual oxygen in the argon, some oxide film may be present even in the argon experiments, which could explain that the estimated critical velocity for A356-argon is slightly higher than the value from Eq. [7]. Using the average jet diameter for the A356 experiments (1.44 cm), and the range of jet velocities spanning all A356 experiments (3.0 to 4.1 m/s), the range of Weber numbers for all A356 experiments is found to be 350 to 653. Finally, for the A356-argon experiments with a 33 cm nozzle height, it was assumed that air entrainment was occurring throughout the experiment. The Weber number for the lowest jet velocity for that case (3.5 m/s) is 476. Comparing that with the value of 300 from Eq. [7],[11] that assumption is strongly supported.

## V. CONCLUSIONS

A measurement system was developed to measure gas entrainment for a plunging jet of aluminum alloy A356. The system operation and accuracy were verified by gas entrainment experiments using water, where the results agreed well with a published entrainment correlation. For air and argon atmospheres the measured entrainment results for water are the same. Experiments using hot water demonstrate the importance of correcting the entrained gas temperature. The temperature of the gas collected during the experiment is measured and used for this correction. Experiments were performed for a plunging jet of liquid A356 in argon and air atmospheres using three nozzle heights. The effects of oxidation on air entrainment and the inception point are presented by comparing results from argon and air. Gas entrainment ratios for the A356 experiments using air atmosphere were lower than in an argon atmosphere. The oxygen content in the entrained air was reduced by about 50 pct due to oxidation, but this does not explain the lower entrainment ratios for air compared to argon. The differences are attributed to a change in the critical jet velocity for entrainment onset between the gases. The critical jet velocity for A356 in ambient air is estimated to be 3.9 m/s with a lower bound of 3.7 m/s, and in argon it is 3.4 m/s with a lower bound of 3.2 m/s. The finding for A356-argon is strongly supported by a previously developed Weber number correlation.[11] It gives a critical velocity of 3.21 m/s using A356 properties and the average jet diameter from the experiments, and for water properties a lower value of 1.4 m/s. The higher critical velocity for A356-air is attributed to the oxide film on the jet surface. All negligibly small entrainment ratios measured are due to the jet impact velocities below the critical value during some or all of the experiment duration. The measured entrainment ratios for air are lower than for argon because of the higher critical velocity for A356-air. For A356-argon at the 33 cm nozzle height, entrainment occurred throughout the experiment duration. The high entrainment ratio measured for this case indicates that gas entrainment at the same jet Froude number for A356 without oxidation is as large as or larger than that for water. These experiments shed considerable light on air entrainment during pouring of A356 but further research is needed. Additional experiments for a larger range of jet velocities, at velocities below entrainment inception using inert atmospheres, and for air at higher velocities above inception over the entire experiment duration. In addition, experiments measuring air entrainment in other metals, such as steel, would be valuable.

**Table IV. Fluid Properties Used to Calculate Critical Velocities**

| Fluid | Surface Tension, $\sigma$ (N/m) | Density, $\rho$ (kg/m$^3$) |
|---|---|---|
| A356 | 0.889[18] | 2400[14] |
| Water | 0.073[19] | 996 |

## ACKNOWLEDGMENTS

The authors wish to thank David Weiss, Dan Hoefert, and the rest of the team at Eck Industries for providing the use of their foundry and support during the aluminum experiments. F.V. Guerra acknowledges CONACYT for the scholarship provided to him during his postdoctoral work at the University of Iowa and the Metallurgical and Materials Research Institute of the Universidad Michoacana de San Nicolás de Hidalgo for supporting the application. This American Metalcasting Consortium (AMC) project is sponsored by the Defense Logistics Agency Troop Support, Philadelphia, PA and the Defense Logistics Agency Information Operations, J68, Research & Development, Ft. Belvoir, VA.

## REFERENCES


1. H. Chanson: Hydraulics of Dams and River Structures, 2004, London, England, pp. 3–15.
2. H. Chanson: *J. Hydraul. Res*., 2013, vol. 51 (3), pp. 223–43.
3. D.A. Ervine, E. McKeogh, and E.M. Elsawy: *Proc. Inst. Civ. Eng*., 1980, vol. 69 (2), pp. 425–45.
4. K.J. Sene: *Chem. Eng. Sci*., 1998, vol. 43, pp. 2615–23.
5. D.A. Ervine and A.A. Ahmed: Paper E1, International Conference on Hydraulic Modeling of Civil Engineering Structures, Coventry, England, 1982.
6. T. Brattberg and H. Chanson: Chem. Engineering Science, 1998, vol. 53(24), pp. 4113-27.
7. E. Van De Sande and J.M. Smith: *Chem. Eng. Sci*., 1976, vol. 31 (3), pp. 219–24.
8. A.K. Biń: *Chem. Engineering Science*, 1993, vol. 48 (21), pp. 3585–30.
9. C. Wanstall, J. Griffin, and C.E. Bates: Paper No. 1.1, Proceedings of the 47th Steel Founders' Society of America (SFSA) Technical and Operating Conference, Chicago, IL, 1993.
10. C.E. Bates and J. Griffin: Research Report No. 106, SFSA Crystal Lake, IL, 1994.
11. J. Ciborowski and A. Bin: *Int. Chem. (Polish)*, 1972, vol. 2, pp. 453–69.
12. R. Gopalan and N.K. Prabhu: *Mater. Sci. Technol*., 2011, vol. 27 (12), pp. 1757–69.
13. J. Campbell: *Complete Casting Handbook: Metal Casting Processes, Techniques and Design*, Elsevier, Oxford, 2011, pp. 19–77.
14. JMatPro, Sente Software Ltd, Surrey Technology Center, Surrey GU2 7YG, United Kingdom.
15. ASME Test Uncertainty, PTC 19.1-2005, American Society of Mechanical Engineering, New York, NY.
16. MAGMAsoft, MAGMA Gmbh, Kackerstrasse 11, 52072 Aachen, Germany.
17. T. Campbell, R.K. Kalia, A. Nakano, and P. Vashishta: *Phys. Rev. Lett*., 1999, vol. 82 (24), pp. 4866–69.
18. J.P. Anson, R.A.L. Drew, and J.E. Gruzleski: *Metall. Mater. Trans. B*, 1999, vol. 30 (6), pp. 1027–32.
19. N.B. Vargaftik, B.N. Volkov, and L.D. Voljak: *J. Phys. Chem. Ref. Data*, 1983, vol. 12 (3), pp. 817–20.